Impact of vacancies and impurities on ferroelectricity in PVD- and ALD-grown HfO₂ films

Cite as: Appl. Phys. Lett. **118**, 032903 (2021); https://doi.org/10.1063/5.0035686 Submitted: 30 October 2020 • Accepted: 02 January 2021 • Published Online: 19 January 2021

🗓 Lutz Baumgarten, 🗓 Thomas Szyjka, 🗓 Terence Mittmann, et al.

COLLECTIONS

Paper published as part of the special topic on Ferroelectricity in Hafnium Oxide: Materials and Devices









ARTICLES YOU MAY BE INTERESTED IN

Polarization switching in thin doped HfO₂ ferroelectric layers

Applied Physics Letters 117, 262904 (2020); https://doi.org/10.1063/5.0035100

Ferroelectricity in hafnium oxide thin films

Applied Physics Letters 99, 102903 (2011); https://doi.org/10.1063/1.3634052

Impact of area scaling on the ferroelectric properties of back-end of line compatible $Hf_{0.5}Zr_{0.5}O_2$ and $Si:HfO_2$ -based MFM capacitors

Applied Physics Letters 118, 062904 (2021); https://doi.org/10.1063/5.0035650

PQBLOX



Shorten Setup Time
Auto-Calibration
More Qubits

Fully-integrated
Quantum Control Stacks
Ultrastable DC to 18.5 GHz
Synchronized <<1 ns
Ultralow noise



100s qubits

visit our website >



Impact of vacancies and impurities on ferroelectricity in PVD- and ALD-grown HfO2 films

Cite as: Appl. Phys. Lett. 118, 032903 (2021); doi: 10.1063/5.0035686 Submitted: 30 October 2020 · Accepted: 2 January 2021 ·







Published Online: 19 January 2021

Lutz Baumgarten,^{1,a)} 🕞 Thomas Szyjka,¹ 🕞 Terence Mittmann,² 🕞 Monica Materano,² 🕞 Yury Matveyev,³ 🕞

Christoph Schlueter, 5 D Thomas Mikolajick, 24 D Uwe Schroeder, 2 D and Martina Müller 5 D

AFFILIATIONS

Note: This paper is part of the Special Topic on Materials and Devices Utilizing Ferroelectricity in Halfnium Oxide.

^{a)}Author to whom correspondence should be addressed: l.baumgarten@fz-juelich.de

ABSTRACT

We investigate the emerging chemical states of TiN/HfO2/TiN capacitors and focus especially on the identification of vacancies and impurities in the ferroelectric HfO₂ layers, which are produced either by physical vapor deposition (PVD) or atomic layer deposition (ALD). Depending on the specific growth conditions, we identify different mechanisms of oxygen vacancy formation. Corresponding spectral features are consistently observed for all HfO2- and TiN-related core levels by hard x-ray photoelectron spectroscopy (HAXPES). In ALDgrown samples, we find spectral signatures for the electronic interaction between oxygen vacancies and nitrogen impurities. By linking the HAXPES results to electric field cycling experiments on the TiN/HfO₂/TiN capacitors, we discuss possible formation mechanisms and stabilization of the ferroelectric HfO2 phase directly related to specific PVD or ALD conditions.

© 2021 Author(s). All article content, except where otherwise noted, is licensed under a Creative Commons Attribution (CC BY) license (http:// creativecommons.org/licenses/by/4.0/). https://doi.org/10.1063/5.0035686

HfO₂ is a key multifunctional material for current device technology. Recently, it is also been successfully used as a ferroelectric or memristive material in nonvolatile memory devices and for novel neuromorphic computing concepts.¹⁻³ Atomic layer deposition (ALD) has become the most widely employed growth process since it allows for a precise thickness control on the level of single atomic layers at CMOS-compatible low deposition temperatures.

However, ALD-grown HfO2 thin films can contain a significant amount of impurities like carbon or nitrogen if the decomposition of the precursor gas in ozone was incomplete or removed ligands readsorb on the surface. The impact of N or C impurities on the HfO2 thin film ferroelectric properties is not fully clarified to date.

As an alternative technique, physical vapor deposition (PVD) by sputtering from an HfO2 target was explored to gain even better control on the stoichiometry and defect concentration in HfO₂ thin films.

Oxygen vacancies are recognized as those defects, which have a positive impact on the stabilization of the ferroelectric orthorhombic phase in undoped HfO₂.⁴⁻⁶ Here, we present a comparative study of both ALD- and PVD-grown HfO2 thin films interfaced with TiN bottom/top electrodes (BE/TEs) integrated into TiN/HfO2/TiN capacitors. We apply hard x-ray photoelectron spectroscopy (HAXPES) as an equally depth-sensitive and element-specific chemical characterization technique, 7,8 which allows us to gain a comprehensive picture of the chemical state of the HfO2 layers. In our analysis, we focus, in particular, on identifying spectral signatures of oxygen vacancies and nitrogen/carbon impurities. We correlate these spectroscopic findings with electrical measurements of the remanent polarization of the ALD- and PVD-grown TiN/HfO2/TiN capacitors. In this way, possible mechanisms of stabilization of the ferroelectric HfO2 phase, resulting from the specific PVD or ALD conditions, are identified.

Sample preparation for PVD and ALD samples is sketched in Fig. 1. For further details, see the supplementary material.

In order to access chemical information from the TiN/HfO2 bottom interface, we performed HAXPES measurements on interstitial areas between the etched TiN top electrodes. The observation of interfacial TiO₂ in the case of PVD (see Fig. 2) arises from the oxygen

¹Forschungszentrum Jülich GmbH, Peter Grünberg Institut (PGI-6), 52425 Jülich, Germany

²NaMLab gCmbH, Noethnitzer Str., 64a, 01187 Dresden, Germany

Deutsches Elektronen-Synchrotron, Notkestraße 85, 22607 Hamburg, Germany

⁴Chair of Nanoelectronic, TU Dresden, 01062 Dresden, Germany

⁵Fachbereich Physik, Universität Konstanz, 78457 Konstanz, Germany

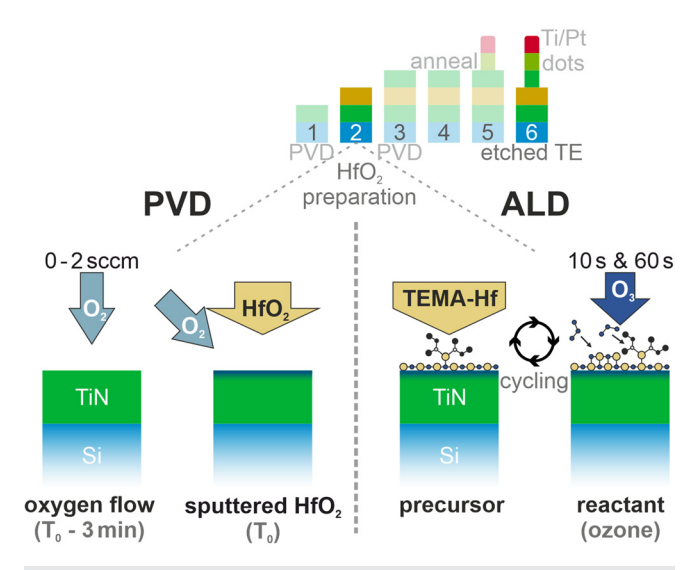


FIG. 1. Process schematics for PVD and ALD of ferroelectric HfO $_2$ in TiN/HfO $_2$ /TiN capacitors: (Left) Using PVD, HfO $_2$ is sputtered in an additional oxygen flow of $\dot{m}=0$ or 2 sccm, respectively. Before the HfO $_2$ evaporation, the O $_2$ flux is stabilized for t=3 min. (Right) Using ALD, layer-by-layer growth of HfO $_2$ is accomplished by an alternating supply (cycling) of TEMA-Hf as the precursor and reactive ozone as the reactant, applying pulse times of $t_{\rm O_3}=10$ and 60 s, respectively.

supply \dot{m} provided before the \dot{m} situ PVD process (see Fig. 1, left). The effective thickness of the TiO₂ intralayer saturates in a self-limiting process at about 3.5 (\pm 0.5) nm. As a consequence, the chemical exchange between the TiN electrode and the HfO₂ is strongly reduced or even suppressed by the TiO₂ intralayer, which serves as a chemical buffer. For the ALD-grown samples, we also observed spectral contributions of interfacial TiO₂ (see Fig. 2). Here, a sizeable surface oxidation is a result of an exposure to air for at least 24 h before ALD growth of HfO₂. Indeed, the TiO₂-related spectral weights of both ALD_{10 s} and ALD_{60 s} samples are comparable to those of the PVD_{2 sccm} sample at

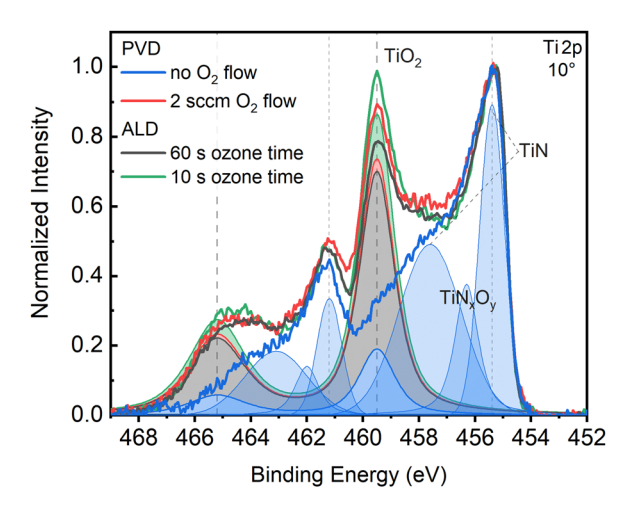


FIG. 2. HAXPES spectra of the Ti 2p core levels for PVD- and ALD-grown samples. An extended interfacial TiO_2 formation is observed for both $\text{ALD}_{10\,\text{s}}$ and $\text{ALD}_{60\,\text{s}}$ samples as well as for $\text{PVD}_{2\text{sccm}}$, but not for the $\text{PVD}_{0\text{sccm}}$ sample. TiO_2 serves as a chemical buffer between the HfO $_2$ and TiN bottom electrode.

 $\dot{m}=2$ sccm. Independent of its chemical origin, however, the ${\rm TiO_2}$ layer serves as a chemical buffer also in ALD-grown samples.

Figure 3 shows the Hf 4f core levels for both sets of PVD- and ALD-grown samples. The intensity is normalized to the Hf $4f_{5/2}$ peak maximum. We find the $PVD_{0\,sccm}$ and $PVD_{2\,sccm}$ Hf 4f peak maxima located at higher binding energies compared to the spectra of both ALD-grown samples. The largest binding energy shift $\Delta E_B=270$ meV is observed between the $PVD_{0\,sccm}$ and $ALD_{10\,s}$ samples. It should be noted that we observe these binding energy shifts between PVD- and ALD-grown samples in all spectral features, which are related to the HfO $_2$ layer (also see the supplementary material). On the other hand, core level features of the TiN electrodes or the TiO $_{2-x}$ interface layer do not show any relative binding energy shift ΔE_B .

Next, we determined the Hf 4f difference spectra relative to the ${\rm ALD_{60\,s}}$ sample (see the supplementary material). They reveal additional Hf 4f contributions at lower binding energies originating from Hf ³⁺, which are attributed to the presence of oxygen vacancies V_0 . ^{9–13} For a quantitative analysis, the Hf 4f spectra were fitted consistently by two doublets. The fits for the Hf ³⁺ contributions are shown as shaded peaks in the lower part of Fig. 3, and the particular Hf ³⁺/Hf ⁴⁺ areal intensity ratios are given in Table I.

As expected, we find a sizeable $\mathrm{Hf^{3+}}$ component for the $\mathrm{PVD_{0\,sccm}}$ sample and only a small one for $\mathrm{PVD_{2\,sccm}}$, while both ALD samples are nearly free of $\mathrm{Hf^{3+}}$. For $\mathrm{ALD_{10\,s}}$, we still find a tiny $\mathrm{Hf^{3+}}$ component that disappears completely after a longer ozone dose in $\mathrm{ALD_{60\,s}}$, in agreement with recent findings. ¹⁴

Figure 4 shows the Hf 4s and O 1s core levels, which have been normalized to the Hf 4s peak. The O 1s peak intensity shows a gradual increase from $PVD_{0\,sccm}$, $PVD_{2\,sccm}$, $ALD_{60\,s}$ to $ALD_{10\,s}$. The O 1s/Hf 4s intensity ratios obtained from an integration over the normalized spectra are given in Table I. For PVD samples, a larger additional oxygen supply leads to a larger oxygen intensity. Moreover, a larger ozone dose $(ALD_{60\,s})$ results in a lower oxygen spectral intensity compared to the $ALD_{10\,s}$ sample.

The O/Hf intensity ratio may decrease for two reasons: First, undesired processes such as the readsorption of organic precursor

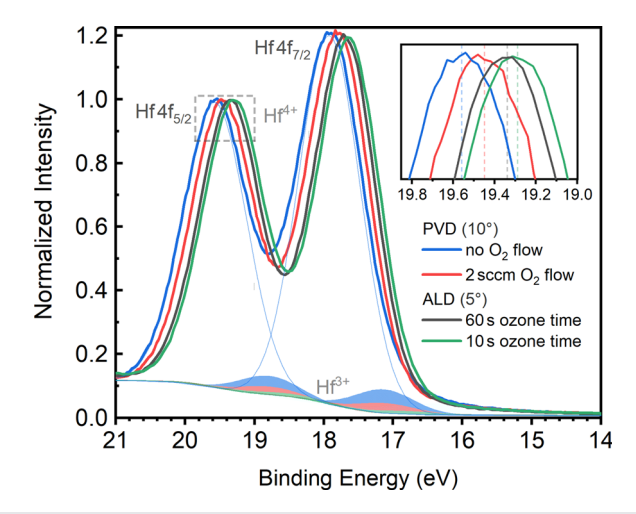


FIG. 3. HAXPES spectra of the Hf 4f core levels for PVD- and ALD-grown samples. The PVD $_{0.2\text{sccm}}$ samples are energetically shifted relative to the ALD $_{10.60\,\text{s}}$ samples. Shaded areas correspond to Hf $^{3+}$ components present in the PVD $_{0.2\text{sccm}}$ samples.

TABLE I. Area intensity ratios Hf^{3+}/Hf^{4+} of the Hf 4f spectra (Fig. 3). Area intensity ratios of O1s, C1s, and the neighboring Hf core levels (Figs. 4 and 5). All values are in %.

	Hf 4f: Hf ³⁺ /Hf ⁴⁺	O 1s/Hf 4s	C 1s/Hf 4d
PVD_{0sccm}	6.2 (±0.2)	1.64	0.18
PVD_{2sccm}	$2.7 (\pm 0.1)$	1.73	0.18
ALD _{60 s}	$0.0~(\pm 0.1)$	1.81	0.50
ALD_{10s}	$0.8~(\pm 0.1)$	1.89	1.24

ligands can likely occur for longer ozone times and may modify the O/Hf ratio in a poorly controllable manner. Second, the relative O/Hf ratio may also decrease by increasing the absolute Hf content, which is most likely the case for the $ALD_{60\,s}$ sample. We note that such large O_3 doses (60 s) are typically not applied in ALD, and we use it here for the purpose of studying the impact of impurities.

Furthermore, the O 1s spectra show a slight increase in intensity at a binding energy of about 533 eV (valley region) for both ALD spectra as compared to PVD. This intensity increase indicates a satellite peak, which is split off from the main O 1s peak by about 1.8 eV (see the supplementary material, Sec. II B). This feature has been discussed in the literature as a signature for an oxygen vacancy V_0 in different oxide materials, $^{15-20}$ with either a 1+ or 2+ valency. 12,13,21

A major difference between ALD- and PVD-grown HfO₂ thin films results from using a metal-organic precursor molecule (TEMA-Hf) in the ALD case. We find clear signatures of C and N impurities incorporated in the ALD-grown HfO₂ films, as discussed in the following.

In Fig. 5, the Carbon C 1s core levels recorded at different photoelectron emission angles are shown for (a) ALD- and (b) PVD-grown samples. All spectra were normalized to the neighboring Hf 4d peaks (not shown). The amount of carbon detected in the PVD-grown HfO₂ layers is, as expected, very low. Moreover, the C 1s peaks do not show any dependence either on the oxygen flow during PVD growth or on the emission angle of the measurement. This finding indicates a homogeneous distribution of carbon impurities within the sample stack, which most likely originates from residuals in the vacuum chamber present throughout the deposition.

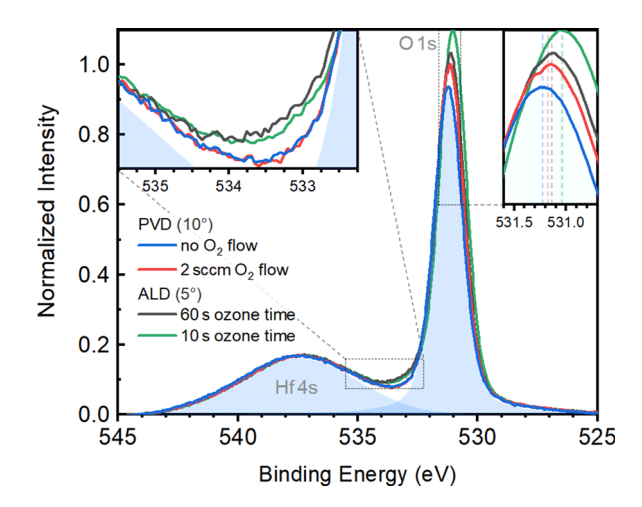
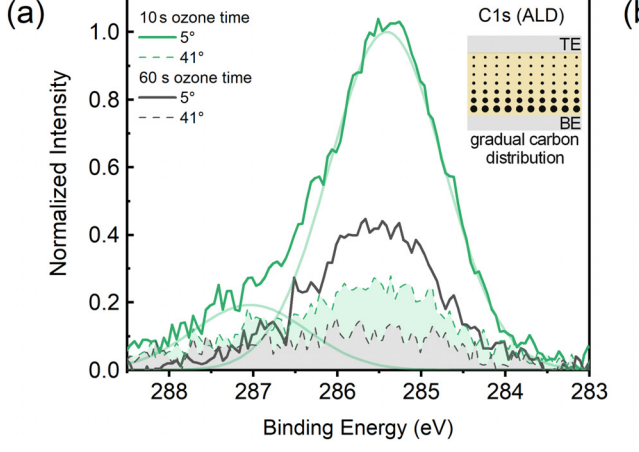


FIG. 4. Normalized HAXPES spectra of the Hf 4s and O 1s core levels for PVD-and ALD-grown samples. (Inset, upper left) The valley region between the Hf 4s and O 1s core level reveals larger intensity for the ALD samples. (Inset, upper right) The peak maximum of the O 1s core level varies for either PVD or ALD-grown samples, respectively.

Clear variations are, however, observable in the C 1s core level of the ALD-grown samples: The C 1s peak intensity is reduced to \sim 40% while increasing the O₃ dosage from 10 to 60 s. Moreover, the C 1s peak intensity shows a strong decrease at a larger surface sensitivity of 41°. Hence, we conclude on an accumulation of carbon impurities toward the bottom TiN electrode [see the inset of Fig. 5(a)]. This finding suggests that the cycled ALD reaction of the TEMA-Hf precursor molecule with O₃ is less effective on a TiO₂ surface, i.e., at the beginning of the HfO₂ growth process, thereby enhancing the amount of organic C residuals in the first HfO₂ layers.

The HAXPES spectra of the nitrogen N 1s core levels, shown in Fig. 6 for (a) ALD and (b) PVD samples, are both dominated by the Ti–N contribution from the bottom electrode and O–Ti–N contribution from the TiN/HfO_2 interface. 9,10 The peak shoulder at



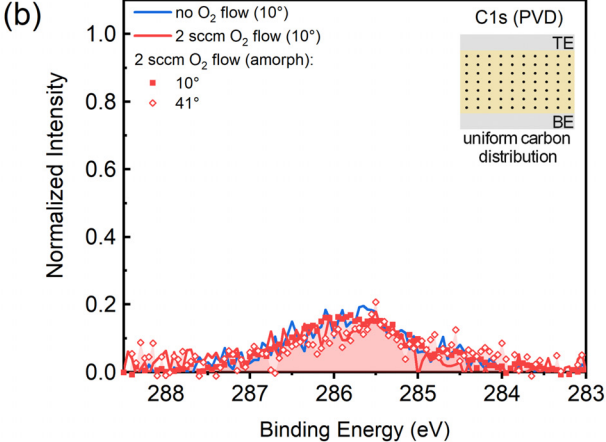


FIG. 5. HAXPES spectra of the C 1s core levels for (a) ALD- and (b) PVD-grown samples. The C content in ALD samples depends on ozone dosage and gradually increases toward the bottom TiN interface. PVD samples show only a very small, uniformly distributed, and growth-independent amount of C impurities.

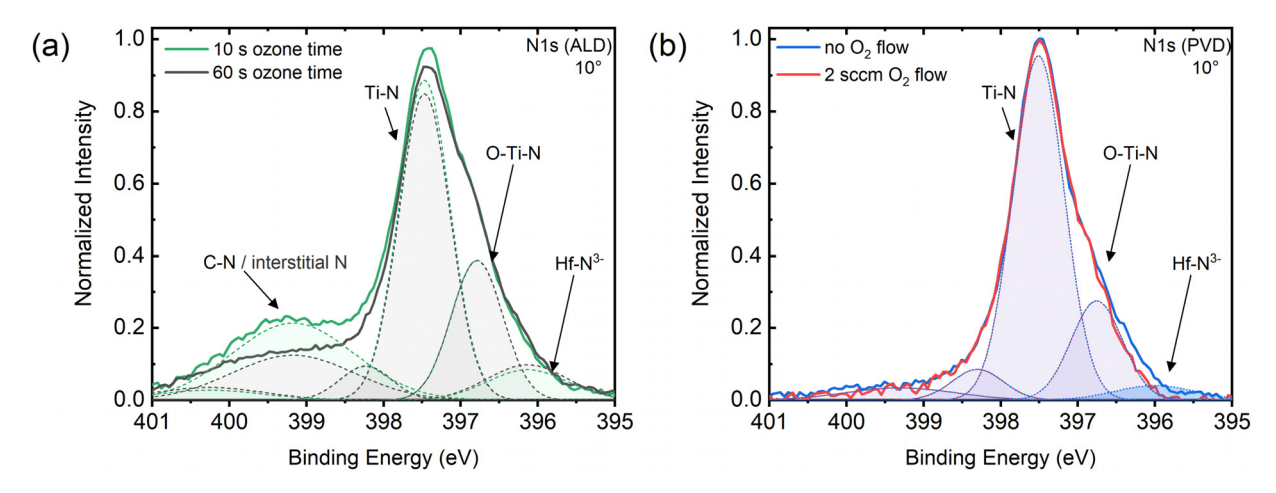


FIG. 6. HAXPES spectra of the N 1s core levels for (a) ALD- and (b) PVD-grown samples, dominated by Ti–N contribution from the bottom electrode and O–Ti–N contribution from the TiN/HfO₂ interface. Hf–N contributions are observed for all samples but PVD_{2sccm}. (a) In ALD samples, C–N or interstitial N decreases with increasing ozone dose, as does the corresponding C 1s spectra in Fig. 5(a).

 E_B = 396 eV is related to Hf⁴⁺-N coordination, ²² whereas the broad emission around E_B = 399 eV to C–N bonds and interstitial Nitrogen contributions. ^{23,24}

In the PVD samples shown in Fig. 6(b), the Hf-N component only appears for PVD $_{0\text{sccm}}$ and is related to an Hf-N formation at the TiN/HfO $_2$ interface, which is suppressed by the TiO $_2$ intralayer formed in PVD $_{2\text{sccm}}$ samples: Since an interface reaction in ALD samples is also protected by a TiO $_2$ layer, the Hf-N component in ALD samples has to be associated with a residual impurity of the ALD process. The same applies to the N component around $E_B = 399\,\text{eV}$ originating from C-N or rather interstitial N. This component shows hardly any angular dependence but is strongly reduced by increasing the O $_3$ dose from 10 s to 60 s. The intensity of the Hf-N component, however, remains basically constant for an increased O $_3$ dose, which indicates a more stable bonding. From its angular dependence (see the supplementary material, Sect. IIC), we conclude on its accumulation at the bottom electrode.

Next, we discuss the experimental observations in terms of the interactions between oxygen vacancies (V_0) and impurities (C or N).

Generally, the ferroelectric phase in HfO_2 can be stabilized by defects. For PVD samples, the oxygen vacancies likely take this function. In HAXPES spectra, oxygen vacancies V_0 manifest themselves as a small Hf^{3+} component at the low binding energy side of Hf^{3+} spectra (see Fig. 3). The Hf^{3+} signature appears, if the two electrons left behind at the vacancy site from a removed neutral oxygen atom are distributed among two neighboring Hf^{4+} atoms.

The reduced $\mathrm{Hf^{3+}}$ component in the $\mathrm{PVD_{2sccm}}$ compared to $\mathrm{PVD_{0sccm}}$ originates from the larger amount of oxygen provided during growth, which fills up the vacancy sites. The emerging ferroelectric properties are fully consistent with this chemical state: Whereas the $\mathrm{PVD_{0sccm}}$ sample is ferroelectric with $\mathrm{2P_{r,10^5}} = 18.2~\mathrm{uC/cm^2}$, see also Fig. 7, the $\mathrm{PVD_{2sccm}}$ sample does not show a significant ferroelectric remanence, as discussed in our previous work.

One might conclude that the absence of the Hf³⁺ component in both ALD Hf 4f spectra (Fig. 3) should result in a reduced ferroelectric remanence. Yet, quite the contrary is the case: Both ALD_{10.860.8}

samples reveal a sizeable remanent polarization with $2P_{r,10^5}^{10s}=13.8$ $\mu\text{C/cm}^2$ and $2P_{r,10^5}^{60s}=11.1$ $\mu\text{C/cm}^2$, respectively. This is remarkable because the O/Hf ratio increases for the ALD samples compared to the PVD samples. Thus, we suggest that the role of the other impurities, i.e., carbon and nitrogen, needs to be taken into closer consideration.

Kim *et al.*²⁴ argued that C impurities can also stabilize the ferroelectric HfO₂ phase, and Rodenbücher *et al.*²⁵ found that a high concentration of oxygen vacancies considerably lowers the formation energy of Hf-C bonds.

However, the C 1s spectra do not show signatures of such an Hf-C contribution, and thus, we rule out a stabilization of the ferroelectric phase in HfO_2 by such a process in the ALD samples.

Rather, we shall discuss the stabilization of the ferroelectric phase by the incorporation of nitrogen impurities into HfO_2 thin films.

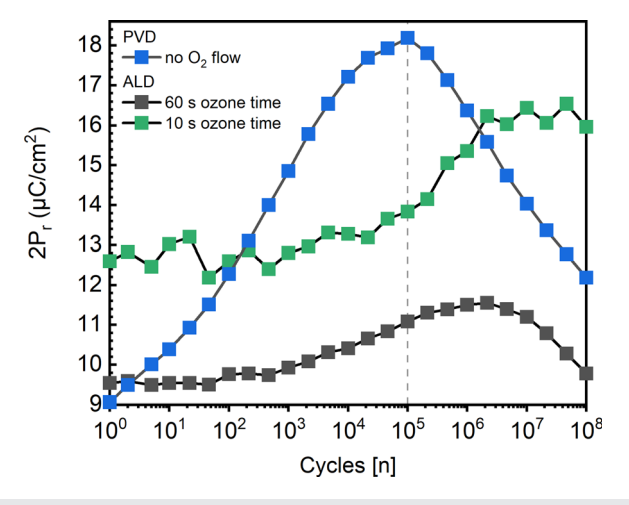


FIG. 7. Electric field cycling behavior of TiN/HfO $_2$ /TiN capacitors, showing the double remanent polarization 2Pr of ALD $_{10\,\text{s}}$, ALD $_{60\,\text{s}}$, and PVD $_{0\text{sccm}}$ samples, which vanishes for PVD $_{2\text{sccm}}$ to 2Pr = 0.

Indeed, nitrogen has been reported both theoretically and experimentally to be the only anion dopant that can stabilize the ferroelectric HfO_2 phase. 26,27 In their *ab initio* models, Umezawa *et al.* 28,29 and Xiong *et al.* 30 proposed an incorporation of nitrogen at the two oxygen nearest neighbor sites of a vacancy. This configuration was found to be energetically most favorable compared to other possible occupation sites for nitrogen, including the vacancy site itself, since two nitrogen will capture both electrons from the oxygen vacancy and form a closed shell VN_2 complex. 28,31,32 Locally, the valencies then amount to V_O^{2+} for the oxygen vacancy site, N^{3-} for nitrogen, and hafnium remains in a Hf^{4+} state.

On the experimental side, Lomenzo *et al.* concluded on the formation of this nitrogen-vacancy complex as an interface reaction at the TaN/HfO₂ interface.³³ In our case, such an interface reaction can be excluded due to the passivation by the TiO₂ interlayer.

This modeling is fully consistent with the HAXPES data of the ALD samples, which reveal vanishing of oxygen vacancy signatures V_0 in the Hf 4f spectra and appearance of stable Hf ⁴⁺-N bonds in the N 1s spectra and vacancy signatures in the O 1s spectra. Moreover, the incorporated N impurities may even compensate the reduced oxygen vacancy density by stabilizing the ferroelectricity in ALD samples. ^{26,27}

Next, we consider the peak shifts of Hf 4f and O 1s toward lower binding energies (Fig. 3). They can be attributed to the decreasing density of oxygen vacancy states within the bandgap. For the PVD samples, this is reflected by the decreasing Hf³⁺ component, caused by the replenishing of vacancy sites by oxygen atoms and the increasing O 1s intensity (Fig. 4). For the ALD samples, the larger shift of Hf 4f toward lower binding energies as compared to the PVD samples can also be attributed to a further decrease in neutral oxygen vacancy states within the bandgap. However, here the N impurities play an additional role in the electronic structure formation. The vacancies are not simply replenished but also electronically passivated by nitrogen impurities, thus forming a VN₂ complex. The former V₀ gap states are now shifted into the valence band.³⁰

As highlighted before, oxygen vacancies are essential for stabilizing the ferroelectric phase in HfO_2 films and also determine the onset of the wake-up effect during electric field cycling of the TiN/HfO₂/TiN capacitors. A key parameter is the mobility of the oxygen vacancies under the application of an electric field. It determines their spacial redistribution and increases the ferroelectric polarization during the wake-up cycling. Hence, a change in the mobility of oxygen vacancies should result in a sizable alteration of the electric wake-up behavior.

In the case of ALD-grown samples, the formation of a vacancy-impurity VN_2 complex should result in a decreased mobility compared to vacancies V_0 in PVD-grown samples, due to the chemical bonding of the oxygen vacancy to the nitrogen impurity. Fully consistent with this assumption, indeed, the electric field cycling behavior of the PVD-grown samples compared to the ALD ones shows an essentially different shape (see Fig. 7). However, the PVD_{0sccm} sample reveals a pronounced increase in the remanent ferroelectric polarization $2P_r$ during wake-up, which may be related to a high mobility of the oxygen vacancies within the HfO_2 layer, like de-pinning of domains pinned to the defect states. Both ALD samples show only a minor increase and a smaller slope of the $2P_r$ curves. Hence, this observation might be related to a decreased mobility of the VN_2 complex formed in the ALD-grown HfO_2 thin films compared to the oxygen vacancies V_0 present in PVD-grown HfO_2 .

In summary, we presented an HAXPES study of TiN/HfO₂/TiN capacitors, for which the ferroelectric HfO2 layers were either prepared by PVD sputtering or by ALD deposition. A comparative picture of the emerging chemical states dependent on the specific PVD or ALD growth conditions was obtained, in particular of the HfO₂ layers. The spectral signatures observed in the Hf 4f, O 1s, and N 1s core levels consistently suggest different mechanisms of oxygen vacancy formation in PVD- and ALD-grown HfO2 thin films and, in the case of ALD, their electronic interaction with nitrogen impurities, which may directly correlate with the HfO₂ ferroelectric properties. By linking the HAXPES results to electric field cycling experiments on the TiN/ HfO₂/TiN capacitors, a novel view on how the stabilization of the ferroelectric HfO2 phase directly relates to specific PVD or ALD growth conditions is provided. Hence, our proposed model may inspire further studies on the complex electronic interactions between oxygen vacancies (V₀) and impurities (C or N) in ferroelectric HfO₂ and their impact on electric characteristics of TiN/HfO₂/TiN capacitors.

See the supplementary material for details about materials growth and crystallization as well as additional ferroelectric and HAXPES results.

This project received funding from the European Union's Horizon 2020 research and innovation programme under Grant Agreement No. 780302. We acknowledge DESY (Hamburg, Germany), a member of the Helmholtz Association HGF, for the provision of experimental facilities. Funding for the HAXPES instrument at beamline P22 by the Federal Ministry of Education and Research (BMBF) under Contract Nos. 05KS7UM1 and 05K10UMA with Universität Mainz; Nos. 05KS7WW3, 05K10WW1, and 05K13WW1 with Universität Würzburg is gratefully acknowledged.

DATA AVAILABILITY

The data that support the findings of this study are available from the corresponding author upon reasonable request.

REFERENCES

- ¹T. S. Böscke, J. Müller, D. Bräuhaus, U. Schröder, and U. Böttger, "Ferroelectricity in hafnium oxide thin films," Appl. Phys. Lett. **99**, 102903 (2011).
- ²A. Rodriguez-Fernandez, C. Cagli, L. Perniola, E. Miranda, and J. Suñé, "Characterization of HfO₂-based devices with indication of second order memristor effects," Microelectron. Eng. 195, 101–106 (2018).
- ³E. Covi, S. Brivio, A. Serb, T. Prodromakis, M. Fanciulli, and S. Spiga, "HfO₂-based memristors for neuromorphic applications," in IEEE International Symposium on Circuits and Systems (ISCAS) (2016), pp. 393–396.
- ⁴T. Mittmann, M. Materano, P. D. Lomenzo, M. H. Park, I. Stolichnov, M. Cavalieri, C. Zhou, C.-C. Chung, J. L. Jones, T. Szyjka, M. Müller, A. Kersch, T. Mikolajick, and U. Schroeder, "Origin of ferroelectric phase in undoped HfO₂ films deposited by sputtering," Adv. Mater. Interfaces 6, 1901528 (2019).
- ⁵M. Pešić, F. P. G. Fengler, L. Larcher, A. Padovani, T. Schenk, E. D. Grimley, X. Sang, J. M. LeBeau, S. Slesazeck, U. Schroeder, and T. Mikolajick, "Physical mechanisms behind the field-cycling behavior of HfO₂-based ferroelectric capacitors," Adv. Funct. Mater. 26, 4601–4612 (2016).
- ⁶R. Materlik, C. Künneth, and A. Kersch, "The origin of ferroelectricity in $Hf_{1-x}Zr_xO_2$: A computational investigation and a surface energy model," J. Appl. Phys. 117, 134109 (2015).
- ⁷M. Müller, S. Nemšák, L. Plucinski, and C. M. Schneider, "Functional materials for information and energy technology: Insights by photoelectron spectroscopy," J. Electron Spectrosc. Related Phenom. 208, 24–32 (2016).

- 8T. Gerber, P. Lömker, B. Zijlstra, C. Besson, D. N. Mueller, W. Zander, J. Schubert, M. Gorgoi, and M. Müller, "Thermodynamic stability and control of oxygen reactivity at functional oxide interfaces: Euo on ITO," J. Mater. Chem. C 4, 1813–1820 (2016).
- ⁹T. Szyjka, L. Baumgarten, T. Mittmann, Y. Matveyev, C. Schlueter, T. Mikolajick, U. Schroeder, and M. Müller, "Enhanced ferroelectric polarization in Tin/HfO₂/Tin capacitors by interface design," ACS Appl. Electron. Mater. 2, 3152–3159 (2020).
- ¹⁰ W. Hamouda, A. Pancotti, C. Lubin, L. Tortech, C. Richter, T. Mikolajick, U. Schroeder, and N. Barrett, "Physical chemistry of the TiN/Hf_{0.5}Zr_{0.5}O₂ interface," J. Appl. Phys. 127, 064105 (2020).
- ¹¹K. Xiong, J. Robertson, M. C. Gibson, and S. J. Clark, "Defect energy levels in Hfo₂ high-dielectric-constant gate oxide," Appl. Phys. Lett. 87, 183505 (2005).
- ¹²P. Broqvist and A. Pasquarello, "Oxygen vacancy in monoclinic HfO₂: A consistent interpretation of trap assisted conduction, direct electron injection, and optical absorption experiments," Appl. Phys. Lett. 89, 262904 (2006).
- ¹³J. L. Gavartin, D. Muñoz Ramo, A. L. Shluger, G. Bersuker, and B. H. Lee, "Negative oxygen vacancies in HfO₂ as charge traps in high-k stacks," Appl. Phys. Lett. 89, 082908 (2006).
- ¹⁴S.-J. Yoon, S.-Y. Na, S.-E. Moon, and S.-M. Yoon, "Polarization switching kinetics of the ferroelectric Al-doped HfO₂ thin films prepared by atomic layer deposition with different ozone doses," J. Vac. Sci. Technol. B 37, 050601 (2019).
- ¹⁵D. J. Loy, P. A. Dananjaya, S. Chakrabarti, K. H. Tan, S. C. W. Chow, E. H. Toh, and W. S. Lew, "Oxygen vacancy density dependence with a hopping conduction mechanism in multilevel switching behavior of HfO₂-based resistive random access memory devices," ACS Appl. Electron. Mater. 2, 3160 (2020).
- ¹⁶S. Jain, J. Shah, N. S. Negi, C. Sharma, and R. K. Kotnala, "Significance of interface barrier at electrode of hematite hydroelectric cell for generating ecopower by water splitting," Int. J. Energy Res. 43, 4743–4755 (2019).
- ¹⁷J.-C. Dupin, D. Gonbeau, P. Vinatier, and A. Levasseur, "Systematic XPS studies of metal oxides, hydroxides and peroxides," Phys. Chem. Chem. Phys. 2, 1319–1324 (2000).
- ¹⁸R. Zhang, H. Huang, Q. Xia, C. Ye, X. Wei, J. Wang, L. Zhang, and L. Q. Zhu, "Role of oxygen vacancies at the TiO₂/HfO₂ interface in flexible oxide-based resistive switching memory," Adv. Electron. Mater. 5, 1800833 (2019).
- ¹⁹Y. Lai, Z. Zeng, C. Liao, S. Cheng, J. Yu, Q. Zheng, and P. Lin, "Ultralow switching current in hfox/zno bilayer with tunable switching power enabled by plasma treatment," Appl. Phys. Lett. 109, 063501 (2016).
- ²⁶C.-Y. Huang, C.-Y. Huang, T.-L. Tsai, C.-A. Lin, and T.-Y. Tseng, "Switching mechanism of double forming process phenomenon in ZrO_x/HfO_y bilayer resistive switching memory structure with large endurance," Appl. Phys. Lett. 104, 062901 (2014).
- ²¹F. P. G. Fengler, R. Nigon, P. Muralt, E. D. Grimley, X. Sang, V. Sessi, R. Hentschel, J. M. LeBeau, T. Mikolajick, and U. Schroeder, "Analysis of performance instabilities of hafnia-based ferroelectrics using modulus spectroscopy and thermally stimulated depolarization currents," Adv. Electron. Mater. 4, 1700547 (2018).

- ²²S. Karwal, M. A. Verheijen, B. L. Williams, T. Faraz, W. M. M. Kessels, and M. Creatore, "Low resistivity HfN_x grown by plasma-assisted ALD with external rf substrate biasing," J. Mater. Chem. C 6, 3917–3926 (2018).
- ²³C. Zheng, G. He, X. Chen, M. Liu, J. Lv, J. Gao, J. Zhang, D. Xiao, P. Jin, S. Jiang, W. Li, and Z. Sun, "Modification of band alignments and optimization of electrical properties of InGaZnO MOS capacitors with high-k HfO_xN_y gate dielectrics," J. Alloys Compd. 679, 115–121 (2016).
- ²⁴K. D. Kim, M. H. Park, H. J. Kim, Y. J. Kim, T. Moon, Y. H. Lee, S. D. Hyun, T. Gwon, and C. S. Hwang, "Ferroelectricity in undoped-HfO₂ thin films induced by deposition temperature control during atomic layer deposition," J. Mater. Chem. C 4, 6864–6872 (2016).
- ²⁵C. Rodenbücher, E. Hildebrandt, K. Szot, S. U. Sharath, J. Kurian, P. Komissinskiy, U. Breuer, R. Waser, and L. Alff, "Hafnium carbide formation in oxygen deficient hafnium oxide thin films," Appl. Phys. Lett. 108, 252903 (2016).
- ²⁶L. Xu, T. Nishimura, S. Shibayama, T. Yajima, S. Migita, and A. Toriumi, "Ferroelectric phase stabilization of HfO₂ by nitrogen doping," Appl. Phys. Express 9, 091501 (2016).
- ²⁷Y. Zhou, Y. Zhang, Q. Yang, J. Jiang, P. Fan, M. Liao, and Y. Zhou, "The effects of oxygen vacancies on ferroelectric phase transition of HfO₂-based thin film from first-principle," Comput. Mater. Sci. 167, 143–150 (2019).
- 28N. Umezawa, K. Shiraishi, T. Ohno, H. Watanabe, T. Chikyow, K. Torii, K. Yamabe, K. Yamada, H. Kitajima, and T. Arikado, "First-principles studies of the intrinsic effect of nitrogen atoms on reduction in gate leakage current through Hf-based high-k dielectrics," Appl. Phys. Lett. 86, 143507 (2005).
- ²⁹N. Umezawa, K. Shiraishi, Y. Akasaka, A. Oshiyama, S. Inumiya, S. Miyazaki, K. Ohmori, T. Chikyow, T. Ohno, K. Yamabe, Y. Nara, and K. Yamada, "Chemical controllability of charge states of nitrogen-related defects in HfO_xN_y: First-principles calculations," Phys. Rev. B 77, 165130 (2008).
- 30 K. Xiong, J. Robertson, and S. J. Clark, "Passivation of oxygen vacancy states in HfO₂ by nitrogen," J. Appl. Phys. 99, 044105 (2006).
- ³¹C. Lee, J. Choi, M. Cho, J. Park, C. S. Hwang, H. J. Kim, and J. Jeong, "Nitrogen incorporation engineering and electrical properties of high-k gate dielectric (HfO₂ and Al₂O₃) films on Si (100) substrate," J. Vac. Sci. Technol., B 22, 1838–1843 (2004).
- ³²J. H. Kim, T. J. Park, M. Cho, J. H. Jang, M. Seo, K. D. Na, C. S. Hwang, and J. Y. Won, "Reduced electrical defects and improved reliability of atomic-layer-deposited HfO₂ dielectric films by *in situ* NH₃ injection," J. Electrochem. Soc. 156, G48 (2009).
- ³³P. D. Lomenzo, Q. Takmeel, C. Zhou, C. M. Fancher, E. Lambers, N. G. Rudawski, J. L. Jones, S. Moghaddam, and T. Nishida, "Tan interface properties and electric field cycling effects on ferroelectric Si-doped HfO₂ thin films," J. Appl. Phys. 117, 134105 (2015).
- ³⁴M. Hoffmann, U. Schroeder, T. Schenk, T. Shimizu, H. Funakubo, O. Sakata, D. Pohl, M. Drescher, C. Adelmann, R. Materlik, A. Kersch, and T. Mikolajick, "Stabilizing the ferroelectric phase in doped hafnium oxide," J. Appl. Phys. 118, 072006 (2015).
- 35S. Starschich, S. Menzel, and U. Böttger, "Evidence for oxygen vacancies movement during wake-up in ferroelectric hafnium oxide," Appl. Phys. Lett. 108, 032903 (2016).